Lab on a Chip

PAPER

View Article Online
View Journal | View Issue

Cite this: *Lab Chip*, 2020, **20**, 3239

Extracellular recording of direct synaptic signals with a CMOS-nanoelectrode array†

Jeffrey Abbott, [abc] Tianyang Ye,[a] Keith Krenek,[a] Rona S. Gertner,[b] Wenxuan Wu,[a] Han Sae Jung,[a] Donhee Ham *[a] and Hongkun Park *[bc]

Received 27th May 2020,
Accepted 29th July 2020

DOI: 10.1039/d0lc00553c

rsc.li/loc

The synaptic connections between neurons are traditionally determined by correlating the action potentials (APs) of a pre-synaptic neuron and small-amplitude subthreshold potentials of a post-synaptic neuron using invasive intracellular techniques, such as patch clamping. Extracellular recording by a microelectrode array can non-invasively monitor network activities of a large number of neurons, but its reduced sensitivity usually prevents direct measurements of synaptic signals. Here, we demonstrate that a newly developed complementary metal-oxide-semiconductor (CMOS) nanoelectrode array (CNEA) is capable of extracellularly determining direct synaptic connections in dense, multi-layer cultures of dissociated rat neurons. We spatiotemporally correlate action potential signals of hundreds of active neurons, detect small (~1 pA after averaging) extracellular synaptic signals at the region where pre-synaptic axons and post-synaptic dendrites/somas overlap, and use those signals to map synaptic connections. We use controlled stimulation to assess stimulation-dependent synaptic strengths and to titrate a synaptic blocker (CNQX: IC_{50} ~ 1 μM). The new capabilities demonstrated here significantly enhance the utilities of CNEAs in connectome mapping and drug screening applications.

Introduction

Understanding how neuronal network activity gives rise to higher functions of the brain has long been one of the most important questions in neuroscience.[1] At the same time, neurological diseases affect more than 1 billion people worldwide,[2] leading to significant efforts to accelerate the pace of neurological drug development.[3,4] In these applications that require functional measurements of synaptic connections, the patch clamp technique remains the dominate tool. Its high-fidelity intracellular interface is capable of measuring small-amplitude post-synaptic potentials (PSPs), thus enabling direct synapse measurement. Its laborious patching process and large size, however, have prevented large network investigations and slowed measurements to <10 synapse connections a day. The act of gaining intracellular access eventually kills the neuron as well, preventing long-term monitoring and experimentation.

Microelectrode arrays (MEAs) measure small spikes in the extracellular solution when a neuron fires an action potential (AP).[5] The extracellular signals are an attenuated time derivative of the intracellular AP signal due to the high-impedance, capacitive properties of the cell membrane. The non-invasiveness of its recording combined with its large spatial coverage using hundreds to thousands of electrodes has made it a standard tool for monitoring neuronal network activity.[5–14] Various techniques are used for analyzing MEA extracellular recordings, including spike-sorting to identify unique neurons,[15] cross-correlation to reveal correlated neuron firings,[16–19] spike-triggered-averaging (STA) to map AP propagations,[12,16,20–22] and peristimulus time histograms (PSTHs) to find network activity correlated to a stimulation.[23,24] Nonetheless, the reduced coupling between neurons and MEAs has prevented direct PSP measurement and therefore direct measurement of single synaptic transmission events.[25] It is important to note that many previous *ex vivo* recordings[21,26–30] have recorded extracellular synaptic signals: unfortunately, such signals could not be used for mapping synaptic connections since they typically represent the sum of many synaptic transmissions.[21]

Recently we have developed complementary-metal-oxide semiconductor (CMOS) nanoelectrode arrays (CNEAs)[31–34] that are capable of both intracellular and extracellular measurements. These devices feature an array of 4096 nanostructured electrodes that enable intracellular access *via* membrane permeabilization, combining the high-fidelity of patch clamping and the network capabilities of MEAs. Such

[a] *School of Engineering and Applied Sciences, Harvard University, Cambridge, MA 02138, USA. E-mail: donhee@seas.harvard.edu*
[b] *Department of Chemistry and Chemical Biology, Harvard University, Cambridge, MA 02138, USA. E-mail: Hongkun_Park@harvard.edu*
[c] *Department of Physics, Harvard University, Cambridge, MA 02138, USA*
† Electronic supplementary information (ESI) available. See DOI: 10.1039/d0lc00553c

access allowed for PSP measurement and high-throughput synapse mapping,[33] but its intracellular nature was invasive just like the patch clamp, thus preventing a long-term recording of the synaptic connectivity.

In this work, we exploit the non-invasiveness of CNEA's extracellular current recording mode to monitor both spontaneous and stimulated network activities. First, we use our CNEA to record spontaneous AP spiking to map not only the AP propagation paths of hundreds of unique neurons, but also to locate potential synapses. We then identify small (~1 pA after averaging) extracellular synaptic signals at the region where pre-synaptic axons and post-synaptic dendrites/somas overlap. The location, in conjunction with the time correlation in cross-correlograms of pre-to-post-synaptic signals, confirms the synaptic origin of the signals and thus direct synaptic connections. Second, we use the CNEA to extracellularly record stimulated activities. Our CNEA allows recording within <1 ms after adjacent electrode stimulation, enabling PSTHs and spike probability over time to be used to identify synaptic connections. Specifically, stimulated synapses exhibit PSTH broadening due to PSP summation jitter and probability decay due to synaptic fatigue. We then use this new synaptic stimulation/measurement technique to titrate the synaptic blocker cyanquixaline (CNQX) and demonstrate its utility for synaptic strength assessment.

The capability to identify synaptic connections *via* extracellular coupling enhances the CNEA's ability for neurological drug screening and connectome mapping applications. Such techniques may also be applicable to other MEA studies *in vitro*, *ex vivo*, or *in vivo*[13,35–37] if similar nanoelectrode–neuron coupling can be achieved: both the tight neuron seal and decreased impedance of the nanoelectrodes help to improve signal transfer in comparison to traditional planar electrodes and to localize the recordings. For example, current MEA-based neuronal assays only assess firing statistics of network-wide activity.[38] Assessing drug's affects at the synapse level, as we demonstrate here, will allow for higher-throughput, higher-information-content assessment for neurological pharmaceutical candidates. Moreover, non-invasive synaptic connection determination opens the door for long-term potentiation[39] and synaptic plasticity[40] studies, two key concepts for understanding the brain and neuronal circuitry whose time scales are longer than what intracellular recording can achieve.

Experimental

Chip design, fabrication, and packaging

We designed the custom CMOS integrated circuit (IC) and outsourced its fabrication in 0.18 μm technology to the United Microelectronics Corporation. Subsequently, we post-fabricated the platinum (Pt) electrodes on the surface aluminum pads of the CMOS IC in house.[33] We used the platinum black (PtB) vertical nanoneedle with pad edge electrodes for all experiments, with the fabrication method described previously.[33] After the electrode post-fabrication, the CMOS ICs were wire-bonded to chip carriers (Spectrum Semiconductor Materials, San Jose, CA). A glass inner and outer ring (Friedrich & Dimmock, Millville, NJ) were glued to the chip and chip carrier, respectively, using polydimethylsiloxane (PDMS). PDMS was then poured between these two glass rings to encapsulate the wire bonds. Neurons were cultured in the well formed by the inner ring once the device was completed.

Neuron culture and drug application

E18 combined rat neurons from the cortex, hippocampus and ventricular zones were purchased from Brainbits LLC (Springfield, Il) and cultured according to the protocols we outlined in our previous work.[33] Half media swaps were performed on the second day of plating and every 3 days afterwards to maintain cell health. Electrical measurements were performed in neuron culture media with or without a Pt reference electrode (we will specify when we used it going forward). All measurements were performed using the mini-incubator setup (ESI† Fig. S3). The temperature of the CMOS IC was set to 34 °C for experiments using the integrated temperature sensors and heater except for the experiments of ESI† Fig. S6 where the temperature was adjusted between 28–36 °C. The devices were cleaned with trypsin, soap water and DI water after each neuron culture and were reused by performing re-deposition of PtB.[33]

For the drug experiment of Fig. 4c, a small amount of drug was added to make 25 μM/10 μM/50 μM APV/CNQX/bicuculline solution. Eight half media exchanges were then performed before the final measurement. For the drug experiment of Fig. 5, small amounts of CNQX were added to form the concentrations stated, and eight half media exchanges were then performed before the final measurement.

Electrical recordings and signal filtering

Data was acquired using LabVIEW software and post-processed using LabVIEW and MATLAB. For the comparison data of Fig. 1d and ESI† S1, 1200 s voltage and current recordings were sequentially performed on a neuronal ensemble cultured 12 days *in vitro* (DIV). Recordings were high-pass filtered using a single-pole 100 Hz filter, and spike detection was performed using only negative polarity spikes. Average spike amplitudes and the spike threshold of 5σ were calculated for pixels measuring more than 50 spikes in both recordings. For the experiments of Fig. 2 and 3, the data processing consisted of transient signal high pass filtering at 200 Hz, spike detection at -3.5σ, spike sorting using amplitude vectors and principal component analysis (PCA)/clustering, and a final cross-correlation step, as outlined in Fig. 2c and ESI† S4. Spike-triggered-averaging (STA) was then performed on the identified unique neurons (*e.g.*, Fig. 2d). For the experiments of Fig. 4 and 5, the window of feedback shorting was first zeroed and the signal was then high-pass

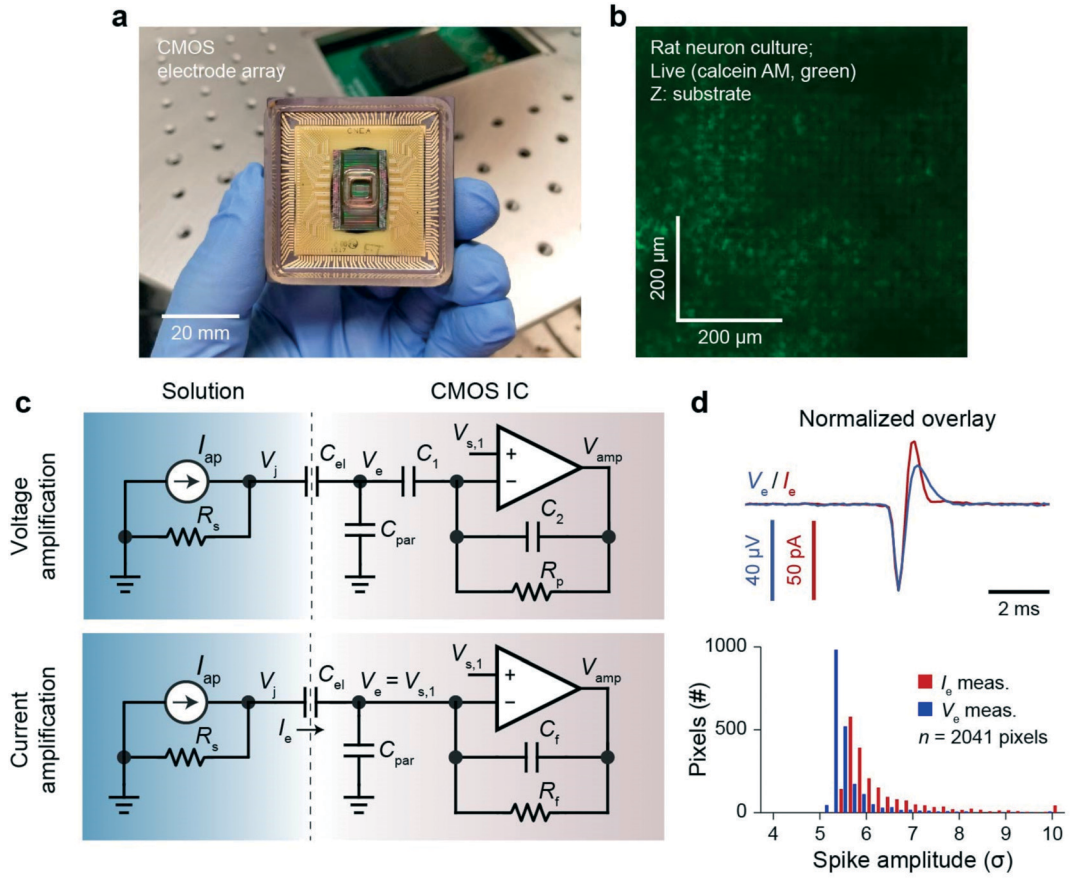

Fig. 1 Extracellular recording of dissociated rat neurons using a CMOS electrode array. a, A CMOS electrode array packaged with a microfluidic well contains 64 × 64 = 4096 pixel pads (20 µm pitch) at its center connected to 4096 amplifiers around its periphery. b, Representative confocal fluorescence microscopy image of a dense dissociated rat neuron culture on a CMOS electrode array used for the electrophysiological experiments. c, The neuron-electrode-circuit model using a voltage amplifier (top) and current amplifier (bottom). The op-amp with output, V_{amp}, amplifies extracellular neuron action potential currents, I_{ap}, which induce junction voltages, V_j, across the electrode seal resistance, R_s. The PtB electrode is modeled by its double layer capacitance, C_{el}, and parasitic line capacitance, C_p = 2 pF. The voltage amplifier uses the ratio of capacitors to set a voltage gain of ~300 V/V and a large feedback resistance of 50 GΩ to set a low-frequency pole of ~100 Hz. The transimpedance current amplifier uses a feedback resistance of 700 MΩ to set its gain, and a feedback capacitance of 100 fF to set a high-frequency pole of ~2 kHz. V_e is biased using a reference voltage, $V_{s,1}$, to set the DC component of the electrode current, $I_{e,DC}$, to 0 A. d, Top, normalized overlay of the voltage and current EAPs from the same electrode/neuron. Bottom, the measured signal-to-noise ratio (SNR) of the measured spikes expressed in standard deviation for voltage and current amplification: the current amplification exhibits higher SNR and is used throughout this manuscript.

filtered using a 50 Hz pole. For subsequent analysis, spike detection was then performed at -5σ to identify EAPs.

Results & discussion

CNEA in the extracellular current recording mode

Our CNEA features 64 × 64 = 4096 independent PtB electrodes spaced at a pitch of 20 µm (ref. 33) (Fig. 1a and b). Beneath each electrode lies a CMOS pixel circuit consisting of stimulation and amplification sub-circuits. Unlike other CMOS MEAs whose underlying pixel circuits implement only high input-impedance voltage amplifiers to record the electrode voltage,[6–14] each pixel circuit in our CNEA can measure electrode voltage (V_e) with a high input-impedance voltage amplifier, or electrode current (I_e) with a low input-impedance current amplifier (Fig. 1c). The signal transfer from the neuron to the amplifier output is similar for both configurations (see ESI† Fig. S1 for simulations): the top of Fig. 1d shows a single-pixel comparison of the voltage and current extracellular AP (EAP) waveforms where the ratio of the peak voltage to current is ~1 MΩ, approximately our estimate of the seal resistance, R_s, in Fig. 1c. We calculate the input-referred current noise of the voltage and current amplification as 10.6 pA_{RMS} and 6.9 pA_{RMS}, respectively, integrated from 0.1 Hz to 100 kHz. The modest improvement of noise performance for the I_e amplification is seen in a comparison of I_e/V_e recordings for 2041 pixels in the bottom of Fig. 1d, where I_e measurements result in higher signal-to-noise ratio (SNR) spikes.

The current-recording configurations offer another major advantage over the voltage recording configuration in that the former does not require a reference electrode. This difference arises from the low-input impedance of the 4096 current amplifiers collectively biasing the extracellular

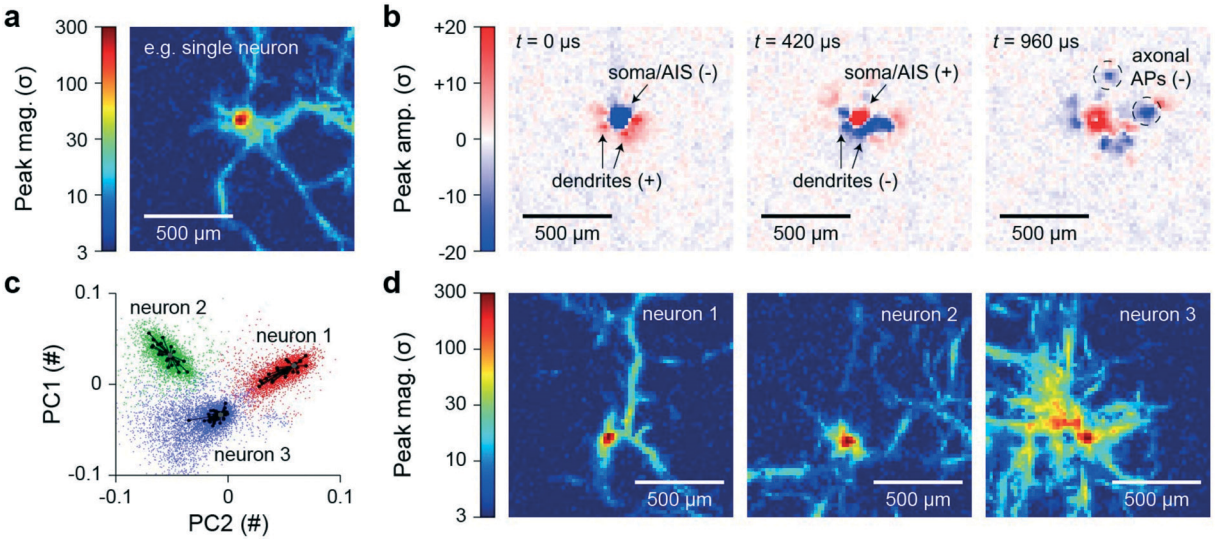

Fig. 2 Mapping and spike sorting neurons and their action potential propagations. a, A rat neuron's electrical imprint on the pixel array is mapped from a 20 min recording and 1800 extracellular spikes using spike-triggered-averaging (STA): the spike magnitude expressed in standard deviation (σ). b, The AP firing is visualized over time (see also ESI† Video S1) and used to identify features of the neuron: the soma/axon initial segment (AIS) is negative and dendrites are positive at t = 0 and reverse polarities at ~400 μs, axonal AP propagations are observed to propagate away from the soma/AIS after the initial AP firing with a mainly negative polarity. c, Principle component (PC) analysis is used for spike sorting to distinguish unique neuron spikes, three neurons are determined for the pixel example. Clustering using sub-clusters (black) are combined following spike density gradients (maximum density, gray) in PC space (ESI,† methods). d, Electrical imprint for each of the three neurons show unique and distinct propagations for confirmation of the clustering.

solution: the impedance of each individual electrode itself is still quite high (~300 kΩ at 5 kHz, or ~100 pF),[33] but the 4096 pixels in parallel reduces the collective impedance to the solution to ~73 Ω at 5 kHz, significantly less than most reference electrode impedances (~100 Ω to 1 kΩ for large reference electrodes). Indeed, our measurements show that removing a large reference electrode from solution only modifies the measured current at 5 kHz by 13% (ESI† Fig. S2). For *in vitro* recordings, elimination of a reference helps to prevent media contamination while also permitting a lid (with a hole for air exchange) to be placed directly over the culture well to prevent evaporation.

Due to these and other stimulation benefits that we discuss in a later section, we use the current-amplification configuration for most of our experiments and present all data as the I_e or the ratio of the signal to the standard deviation noise, σ. For subsequent data analysis after recording, we use a negative threshold of 3.5σ–5σ (23 pA–33 pA) to detect EAP spikes from the soma/axon initial segment of the neuron. Much of the spontaneous recording experiments and analysis that we will discuss may also be applicable to voltage amplification measurements, with the caveat of a slightly reduced signal-to-noise ratio and the need for a low-impedance reference electrode.

Mapping AP propagations in hundreds of neurons

We perform spatial mapping of the neurons *via* their EAP propagations, which we obtain by performing STA on the extracellular recording of spontaneous activities[12,16,20–22] (Fig. 2). Specifically, using an origin neuron's spike time as reference, windows of data around the spike time for each pixel are averaged together to extract correlated signals and reduce uncorrelated noise. Assuming uniform uncorrelated noise, the SNR improves as the square root of the number of windows, $N^{1/2}$. But unlike previous studies which use sparse, single-layer cultures,[12,16,20–22] we plate a large number of neurons to form dense, multi-layer cultures (Fig. 1b and ESI† S3c). This high-density culture produces substantial network activity, which allows thousands of STA windows to be used when it is recorded in full-frame using our CNEA device.

Fig. 2a shows an example neuron on the array identified *via* spatially mapping of EAP propagation (the peak amplitude of the average signals is visualized in the figure). In this single neuron example, 1800 windows are used for the averaging, which increases the SNR by ~40-fold and reduces the 5σ threshold to <1 pA. Different features of the neuron, including the soma/axon initial segment (~50 pA negative spike), dendrites (~1–5 pA positive spike), and axons (~1–5 pA negative spikes) are then identified[5] (Fig. 1b and c). The full time-course of the neuron EAP propagation is shown in ESI† Video S1.

In dense neuron cultures where we record spiking signals from all 4096 pixels, we distinguish unique neurons using spatial oversampling[41] and an amplitude-based principal component (PC) spike-sorting algorithm (Fig. 2c and ESI† S4). The uniqueness of such sorting is confirmed by mapping the electrical imprint of the identified neurons (Fig. 2d). In active cultures, hundreds to thousands of neurons are identified from 20 min recordings (*e.g.* of 2042 neurons in ESI† S4f). The recording of such large numbers of neurons is possible because of the dense cultures and full-frame recording capability of our CNEA. The real-time AP

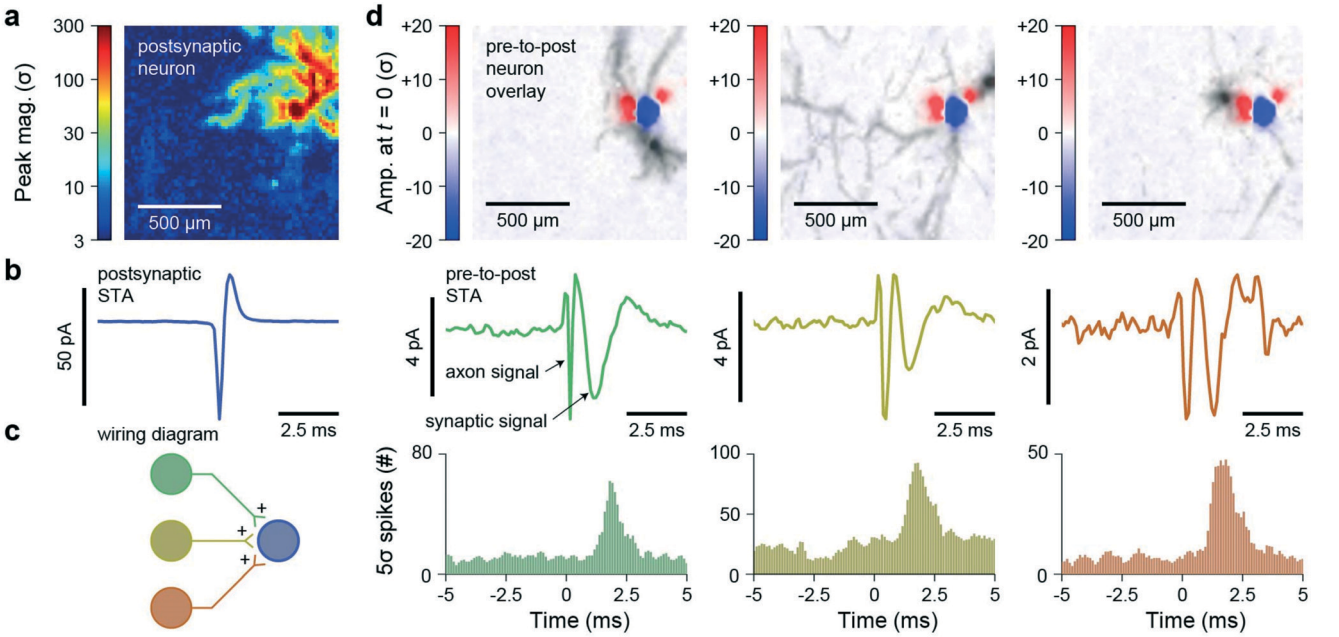

Fig. 3 Mapping synaptic connections using spike-triggered-averaging and cross-correlation. a–c, A post synaptic neuron, with its spike-triggered-average (STA) electrical imprint and soma STA shown in (b), has multiple excitatory synaptic inputs (c). d, Pre-to-post overlays show that the soma/AIS or dendrites of the post-synaptic neuron overlay axon branches from the respective pre-synaptic neurons allowing for synapse formation. The three pre-to-post STA signals each show a synaptic signal following the axon propagation signal which are time correlated with the pre-to-post cross correlograms confirming the direct synaptic connections.

propagation through the networks can be visualized using the neurons' spike times and their average propagations, as shown in ESI† Video S2 for 15 most active neurons and Video S3 for 141 neurons.

Taking advantage of the non-invasive nature of extracellular recording, we track neuronal growth during culture by observing how EAP propagation maps change (expand) over time (ESI† Fig. S5 and Video S4 show measurements of a neuron culture from 8 DIV to 28 DIV, and Fig. S6 and Video S5 show measurements at temperatures from 28–36 °C). As observed previously,[5,38] spiking activity and periodic firing behaviors gradually increase over the weeks with the peak network activity measured at 24 DIV (ESI† Fig. S5a). During this period, individual neurons exhibit significant growth in both the axonal tree and dendritic tree and an increase axonal propagation speed (from 0.23 m s^{-1} at 8 DIV to 0.31 m s^{-1} at 27 DIV along the main axon of the example neuron: ESI† Fig. S5b and Video S4). From these measurements, we determine the optimal culture conditions for our experiments, ~20–30 DIV cultures at 34 °C, where the neurons exhibit large and fast EAP spread and the networks exhibit significant connectivity. We use these conditions in the experiments described in the following sections on synaptic connections.

Finding direct synaptic connections *via* spontaneous activity recording

We now discuss a method to identify direct synaptic signals from the extracellularly recorded spontaneous activity data. We first use cross-correlation of EAP spiking to find a pair of neurons whose activities are correlated with each other.[16–19,25] The cross-correlogram is calculated as the binning of the time difference between two neuron's spike times for all pair of neurons identified. EAP cross-correlograms reflect an excitatory synapse when a low-latency peak is observed:[16–19,25] the onset time of the peak reflects the pre-synaptic axonal propagation delay and subsequent synaptic cleft delay while the breath of the peak signifies the time jitter associated with PSP summation to threshold. It is important to note that such "synaptic" correlograms are not by themselves definitive indicators of direct synaptic connection because a similar histogram shape can be produced *via* a common synaptic input to both neurons (*e.g.*, see ESI† Fig. S7).

To distinguish direct synaptic connections from indirect correlations, we investigate the spatial overlap region of neurons' axonal and dendritic trees[16] and look for signals related to the direct synaptic connection. We find a specific indicator of a synaptic connection in the STA of pre-synaptic neurons as a second peak following the axonal propagation signal that is longer in duration (~1–2 ms) and on the same order of magnitude (Fig. 3). These synaptic signals are confined to ±40 µm along the axon propagation direction and ±30 µm perpendicular to the axon (measured amongst a 5 × 4 group of pixels, ESI† Fig. S8), which is a typical spread of an extracellular signal from an axon (diameter on the order of ~1 µm). This observation indicates a localized source of the signal, which may be either due to Ca^{2+} influx at a pre-synaptic terminal, induced post-synaptic ion-channel currents, or a combination of both. The time-course of the

signal is similar to the kinetics of the Ca^{2+} presynaptic influx.[42] It could also reflect a time-filtered postsynaptic potential similar to the filtering of an intracellular AP to an EAP. Regardless of the pre-synaptic *versus* post-synaptic origin, the time correlation of the signal immediately before the onset of the peak in the cross correlograms indicates that it is directly related to the synapse (Fig. 3d). We note the synaptic signal shown in Fig. 3 does not originate the post-synaptic neuron's EAP: the effects of the post-synaptic EAP on the pre-synaptic STA is comparatively smaller and appear later than the synaptic signal, as shown in ESI† Fig. S9.

Extracellular signals related to synapses have been observed previously in *ex vivo* slice experiments.[21,26–30] These *ex vivo* signals, which are observed upon extracellular stimulation of the neural activities, have a typical amplitude of >1 mV[21,26–29] and durations exceeding 10 ms.[21,27–29] Importantly, the dispersed spatial propagation of these signals indicate that they represent the sum of many synaptic transmission events.[21] In contrast, the average synaptic signals reported here, with their small-amplitude (~1–4 pA, or equivalently ~1–4 μV: see Fig. 1 for the current-to-voltage conversion), short durations (~1 ms), and localized locations (<100 μm spread) are likely due to single-synapse transmission events from pre-to-post synaptic neurons. As such, the measurements presented here are more similar to proximate extracellular synaptic current measurements performed with a patch clamp.[43] The ability to measure such a localized synaptic transmission derives from the high spatial density of our electrode array and the thousands of STA windows used to improve signal-to-noise ratio for detecting neuron-specific, correlated, ~1 pA/1 μV signals. In comparison to post-synaptic intracellular measurement techniques that measure all post synaptic potentials/currents, the extracellular synaptic signals we measure here are limited to single pre-to-post neuron connections. Therefore, our STA-based mapping technique may prove more useful in studying synaptic transmission than describing the transient activities of a neuron.

Extracellular stimulation and recording

Beyond spontaneous recording, the current amplification of the CNEA can be paired with stimulation for more controlled probing of direct synaptic connections. For such experiments, amplifiers are arranged in a buffer configuration (switches in their feedback loops closed[7,9]) during the stimulation to prevent amplifier saturation (Fig. 4a). As we transition from stimulation to recording phase, the feedback switches are opened, and the amplifiers change from the buffer mode to the amplification mode quickly, enabling extracellular current recording from electrodes adjacent to stimulation electrodes within less than 1 ms after the stimulation pulse is applied (Fig. 4b). In comparison, the CNEA's voltage amplification mode requires at least 10 ms of settling to become unsaturated due to its high impedance configuration. Previous voltage-amplifier-based studies have the saturation time as small as ~5 ms,[20] but still miss much of the stimulated activities, as we will show in the following experiments. It is important to note that, unlike the traditional microelectrode array measurements that employ a global reference electrode, the low impedance biasing of the non-stimulated electrodes act as local references for return currents in our experiment (see ESI† Fig. S2 for a measurement of such return current distribution).

We use a repeated 0.6 V amplitude, 200 μs, biphasic voltage signal for neuronal stimulation (Fig. 4a). As shown in ESI† Video S6, upon application of thousands of repeated stimulations on a particular pixel, multiple EAP propagations that are time synchronized to the stimulation are induced in the high-density cultures: axons near the stimulation electrode are triggered to fire APs, which then propagate both orthodromically and antidromically.[20] For most experiments, we chose to apply stimulations to eight or more electrodes spread across the perimeter of our CNEA in order to excite many neurons and their processes across the network: an example of 15 electrode stimulation is shown in ESI† Video S7.

The large amount of activity, time-synchronized to the stimulation, makes individual neuron propagations difficult to isolate and map based on averaging alone. To map synapses, we instead leverage our ability to record EAP spikes <1 ms after stimulation. Specifically, we generate PSTHs immediately after the stimulation by binning EAP spikes *via* their time lag to the stimulus (Fig. 4c, bottom). We also calculate spike probability over time by averaging the EAP spike count during a stimulation window period (either 0 or 1) over a rolling window of 2 s (Fig. 4c, top). Different types of connections are then revealed: these include no stimulation/connection, direct stimulations, and stimulated synapses. The examples shown in Fig. 4c consist of three measurements for verification: an initial measurement, a second measurement with synaptic blockers, and a third measurement after washout, each sequentially performed with 1 hour of recovery time and a window period of 50 ms.

A direct stimulation (Fig. 4c, middle) shows a high spike probability over time and a very sharp (<300 μs) histogram width[44] and is immune to synaptic blockers: these observations all indicate that an axon branch is stimulated and APs antidromically propagate to the neuron's soma. In comparison, stimulated synapses (Fig. 4c, right) show an initial high spike probability that declines over time and a broad histogram width (~1–10 ms). Importantly, the signal propagation disappears upon the application of synaptic blockers, confirming its synaptic origin. The broad histogram is the result of the summation of PSPs, which adds a jitter to the time-response of the measured post-synaptic AP. The declining probability over time is indicative of synaptic fatigue: with repeated stimulations, the pre-synaptic terminal becomes exhausted of synaptic vesicles,[45,46] resulting in a vanishing PSP amplitude and therefore a lower probability of AP firing (Fig. 4c and ESI† S10). We note that the preceding discussion focuses primarily on chemical synapses which are

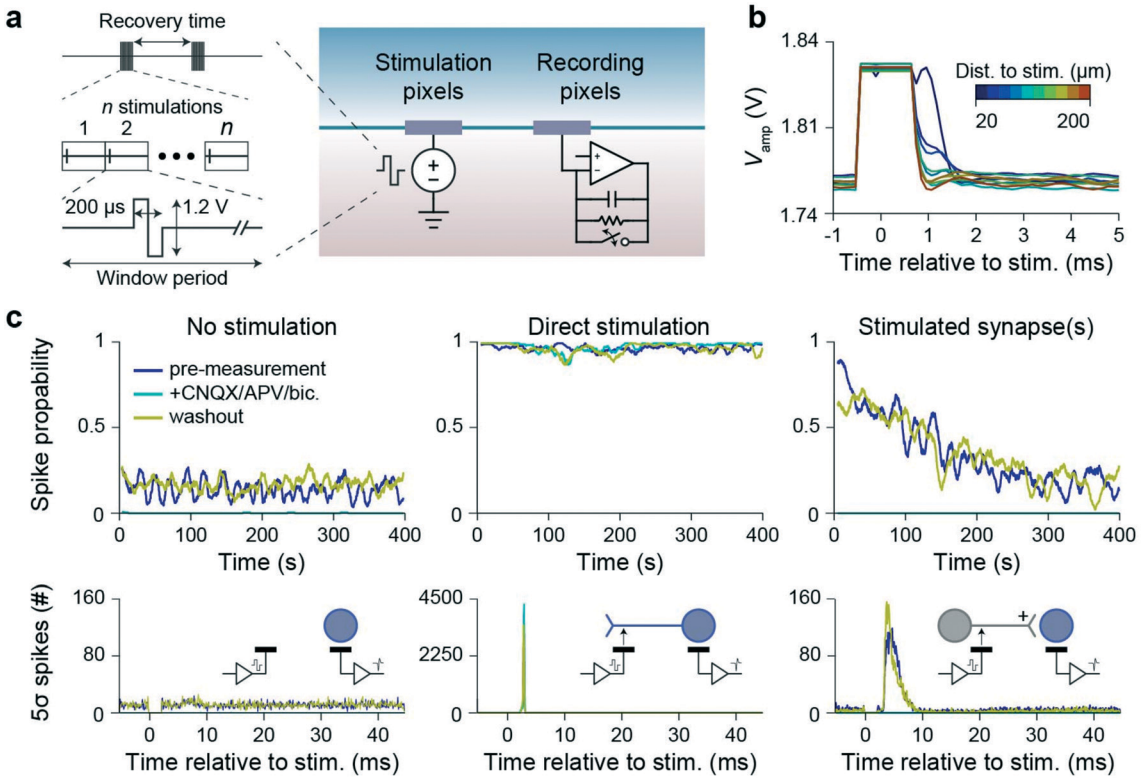

Fig. 4 Stimulation of neurons and their synaptic connections. a, The pixel circuit configurations used for stimulation and recording of neurons. A biphasic voltage signal is repeatedly applied to stimulation pixels while the remaining pixels record. A switch in the feedback of the recording amplifier prevents saturation during stimulation and keeps V_e biased at a constant voltage before, during, and after the stimulation/shorting to help prevent long time constants associated with the electrode. b, Amplifier responses for the utilized shorting duration (feedback shorted during stimulation to +640 µs afterwards). The shorting prevents amplifier saturation and allows for signal recording <1 ms after stimulation. c, To reveal various types of connections during the repeated stimulations, EAP spike detection is performed on recording pixels. Three measurements are shown: an initial, with synaptic blockers, and after washout, each sequentially performed with 1 hour (3600 s) of recovery time, n = 8000 stimulations, and a window period of 50 ms, as defined in (a). The probability of an EAP spike over time (top) and a histogram of the spikes during the stimulation window (bottom, bin size 100 µs) are shown for each type of connection: a direct stimulation, stimulated synapse(s), and no stimulation.

the main type of synapses we observe in our dissociated rat neuron cultures. Electrical synapses could also be stimulated and measured using the PSTH and AP probability over time but would not respond to the addition of chemical synaptic blockers.

Stimulated activity recording – drug screening application

Previous studies have often used PSTHs to measure the effects of stimulation on neuronal networks,[23,24] but little focus has been placed on the short time interval immediately after the stimulation because of the stimulation artifacts/saturation and the ambiguity between direct stimulations and stimulated synapse(s). Our ability to accurately measure EAP PSTHs and the EAP probability over time, which has not been reported previously, grants additional information to distinguish connection types. Furthermore, the stability of the synapse stimulation and measurement also enables synaptic drug screening. For illustrative purposes, we demonstrate this capability in Fig. 5 by showing the effect of an AMPA synaptic blocker (CNQX) on the spike probability over time and correlogram amplitude (Fig. 5). In this experiment, stimulations are applied around the peripheral of the array (Fig. 5a, magenta), and we identify AMPA-synaptically connected pixels (Fig. 5a, blue) using a decaying spike probability over time and a broad histogram that respond to the CNQX titration (Fig. 5b). Both the spike probability over time and PSTH respond to the increasing blocker concentration, with the number of total spikes correlating well with the synaptic strength (Fig. 5c). The half activity concentration of 1.12 µM determined by the total number of spikes from 50 synaptic pixels (Fig. 5d) agrees well with previous studies,[47] highlighting the unique capability of the CNEA in assessing the drug efficacy using primary mammalian synapses.

Conclusions

In this work, we presented CNEA-based experiments and analyses for extracellularly measuring and stimulating neurons and their synaptic connections. Large-scale neuron EAP mapping and measurement of extracellular synaptic signals can be useful for connectome mapping of neuronal networks *in vitro*, *ex vivo*,[21,26–28,30] and *in vivo*[13,35–37] where

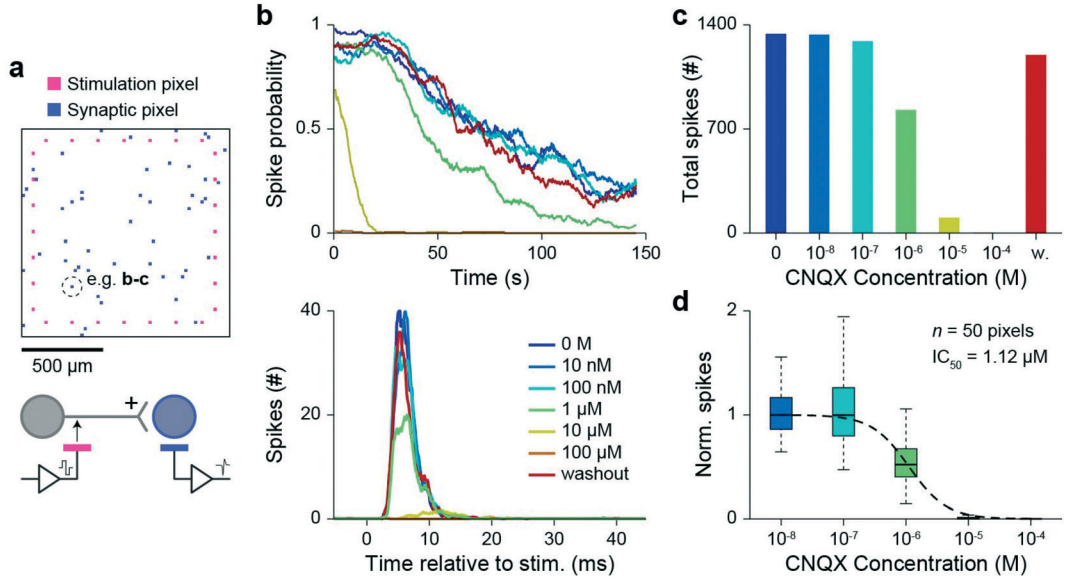

Fig. 5 Synaptic blocker (CNQX) titration. a, Extracellular stimulation of selected pixels (magenta) excite synapses of measured extracellular neurons (blue). b, The probability over time (top), and spike histogram (bottom) are affected by the titration of CNQX, a synaptic blocker, across several orders of concentration and a subsequent washout. A window period of 50 ms and a recovery time of 600 s were used for the experiment. c, The total number of spikes reflects the drug's concentration for the example pixel in (b). d, Changes to the number of spikes across 50 synaptic pixels reveals the concentration dependence of CNQX with a calculated half maximal inhibitory concentration, $IC_{50} \sim 1$ μM.

recent trends have aimed for increasing the number of recording channels and electrodes. Previously, extracellular measurements alone couldn't be used to identify direct synaptic connections because of the unreliable nature of cross-correlograms.[25] We show here that we can measure direct extracellular synaptic signals at the region where pre-synaptic axons and the post-synaptic soma/dendrites overlap and we can use the information to map the paths of neuronal signal propagation both spatially and temporally. If the origin of the extracellular signal is post-synaptic, it may be also be useful for measurement of the synaptic strengths to calculate network weights, because its extracellular magnitude should reflect that of the corresponding intracellular post-synaptic potential. Similarly, inhibitory post synaptic potentials should, in theory, be able to be measured, although we do not observe any inhibitory cross-correlograms in our data to validate such measurement, potentially reflecting synapse expression profiles of our dissociated rat neuron cultures. It is also important to note that our CNEA may fail to extracellularly measure PSPs with reversal potentials close to or at the resting potential, because no change of membrane potential is induced and therefore no extracellular currents would be generated. Non-invasively monitoring of direct synaptic connectivity can be used for long-term studies of neural network development, important for understanding the changes of synaptic strengths over time, as in long-term potentiation[39] and synaptic plasticity.[40]

The repeated stimulation protocols coupled with fast (<1 ms) measurement capability upon stimulation enables PSTHs and spike probability over time to be used to differentiate direct neuron stimulations and synaptic stimulations. The repeatability of such synaptic stimulations enables drug screening for synaptic transmission: in this study, we used the capability to titrate synaptic blocker. Such measurements using a chip-scale device should be useful for high-throughput drug screening technologies, especially those targeting mammalian neurons where current methods of measuring synapse transmission, *i.e.* the patch clamp, are extremely slow and laborious. Likewise, changing stimulation parameters such as the recovery time between stimulations and the period of stimulations enables the probing of synaptic fatigue and pre-synaptic vesicle recycling processes. Such synapse transmission assessments extend the amount of extracted information beyond current MEA-based drug screening that uses network-level responses.[38] Furthermore, pairing such direct synapse stimulations with other known modifiers of synaptic transmission strength, such as spike timing dependent protocols (STDP), could open new insights into synaptic transmission and potentiation, especially if applied to *ex vivo* tissue slices or *in vivo*.

Author contributions

H. P., D. H., J. A., T. Y., and K. K. conceived and designed the experiments. J. A. designed the electronics, T. Y. and K. K. performed post-fabrication and device packaging, J. A., T. Y., K. K., and R. G. performed the experiments, and J. A., T. Y., K. K., H. J., W. W., D. H., and H. P. analyzed the data. H. P. and D. H. supervised the project. J. A., T. Y., K. K., D. H., and H. P. wrote the manuscript, and all authors read and discussed it.

Conflicts of interest

There are no conflicts to declare.

Acknowledgements

Post-fabrication and characterization were performed, in part, at the Center for Nanoscale Systems at Harvard University. The authors are grateful for the support of this research by Samsung Advanced Institute of Technology, Samsung Electronics, Suwon, Republic of Korea (A37734 to D. H. and A37738 to H. P.), Catalyst foundation, Valhalla, NY (J. A., H. P., and D. H.), the Army Research Office (W911NF-15-1-0565 to D. H.), the Army Research Office (W911NF-17-1-0425 to D. H.), the National Science Foundation Graduate Research Fellowship Program (DGE1745303 to K. K.), the Gordon and Betty Moore Foundation (to H. P.), and the U. S. Army Research Laboratory and the U. S. Army Research Office (W911NF1510548 to H. P.).

Notes and references

1 G. Buzsáki, *Nat. Neurosci.*, 2004, **7**, 446–451.
2 World Health Organisation.
3 D. E. Pankevich, B. M. Altevogt, J. Dunlop, F. H. Gage and S. E. Hyman, *Neuron*, 2014, **84**, 546–553.
4 A. Farkhondeh, R. Li, K. Gorshkov, K. G. Chen, M. Might, S. Rodems, D. C. Lo and W. Zheng, *Drug Discovery Today*, 2019, **24**, 992–999.
5 M. E. J. Obien, K. Deligkaris, T. Bullmann, D. J. Bakkum and U. Frey, *Front. Neurosci.*, 2015, **9**, 423.
6 B. Eversmann, M. Jenkner, F. Hofmann, C. Paulus, R. Brederlow, B. Holzapfl, P. Fromherz, M. Merz, M. Brenner, M. Schreiter, R. Gabl, K. Plehnert, M. Steinhauser, G. Eckstein, D. Schmitt-Landsiedel and R. Thewes, *IEEE J. Solid-State Circuits*, 2003, **38**, 2306–2317.
7 F. Heer, S. Hafizovic, W. Franks, A. Blau, C. Ziegler and A. Hierlemann, *IEEE J. Solid-State Circuits*, 2006, **41**, 1620–1629.
8 L. Berdondini, K. Imfeld, A. Maccione, M. Tedesco, S. Neukom, M. Koudelka-Hep and S. Martinoia, *Lab Chip*, 2009, **9**, 2644.
9 U. Frey, J. Sedivy, F. Heer, R. Pedron, M. Ballini, J. Mueller, D. Bakkum, S. Hafizovic, F. D. Faraci, F. Greve, K. U. Kirstein and A. Hierlemann, *IEEE J. Solid-State Circuits*, 2010, **45**, 467–482.
10 R. Huys, D. Braeken, D. Jans, A. Stassen, N. Collaert, J. Wouters, J. Loo, S. Severi, F. Vleugels, G. Callewaert, K. Verstreken, C. Bartic and W. Eberle, *Lab Chip*, 2012, **12**, 1274.
11 M. Ballini, J. Muller, P. Livi, Y. Chen, U. Frey, A. Stettler, A. Shadmani, V. Viswam, I. L. Jones, D. Jackel, M. Radivojevic, M. K. Lewandowska, W. Gong, M. Fiscella, D. J. Bakkum, F. Heer and A. Hierlemann, *IEEE J. Solid-State Circuits*, 2014, **49**, 2705–2719.
12 J. Müller, M. Ballini, P. Livi, Y. Chen, M. Radivojevic, A. Shadmani, V. Viswam, I. L. Jones, M. Fiscella, R. Diggelmann, A. Stettler, U. Frey, D. J. Bakkum and A. Hierlemann, *Lab Chip*, 2015, **15**, 2767–2780.
13 J. J. Jun, N. A. Steinmetz, J. H. Siegle, D. J. Denman, M. Bauza, B. Barbarits, A. K. Lee, C. A. Anastassiou, A. Andrei, Ç. Aydin, M. Barbic, T. J. Blanche, V. Bonin, J. Couto, B. Dutta, S. L. Gratiy, D. A. Gutnisky, M. Häusser, B. Karsh, P. Ledochowitsch, C. M. Lopez, C. Mitelut, S. Musa, M. Okun, M. Pachitariu, J. Putzeys, P. D. Rich, C. Rossant, W. L. Sun, K. Svoboda, M. Carandini, K. D. Harris, C. Koch, J. O'Keefe and T. D. Harris, *Nature*, 2017, **551**, 232–236.
14 D. Tsai, D. Sawyer, A. Bradd, R. Yuste and K. L. Shepard, *Nat. Commun.*, 2017, **8**, 1802.
15 F. Franke, D. Jäckel, J. Dragas, J. Müller, M. Radivojevic, D. Bakkum and A. Hierlemann, *Front. Neural Circuits*, 2012, **6**, 105.
16 T. Bullmann, M. Radivojevic, S. T. Huber, K. Deligkaris, A. Hierlemann and U. Frey, bioRxiv, 2017, pp. 1–23.
17 A. Maccione, M. Garofalo, T. Nieus, M. Tedesco, L. Berdondini and S. Martinoia, *J. Neurosci. Methods*, 2012, **207**, 161–171.
18 P. Barthó, H. Hirase, L. Monconduit, M. Zugaro, K. D. Harris and G. Buzsáki, *J. Neurophysiol.*, 2004, **92**, 600–608.
19 A. Peyrache, N. Dehghani, E. N. Eskandar, J. R. Madsen, W. S. Anderson, J. A. Donoghue, L. R. Hochberg, E. Halgren, S. S. Cash and A. Destexhe, *Proc. Natl. Acad. Sci. U. S. A.*, 2012, **109**, 1731–1736.
20 D. J. Bakkum, U. Frey, M. Radivojevic, T. L. Russell, J. Müller, M. Fiscella, H. Takahashi and A. Hierlemann, *Nat. Commun.*, 2013, **4**, 2181.
21 M. Shein-Idelson, L. Pammer, M. Hemberger and G. Laurent, *Nat. Methods*, 2017, **14**, 882–890.
22 M. E. J. Obien, A. Hierlemann and U. Frey, *Sci. Rep.*, 2019, **9**, 1–19.
23 G. Shahaf and S. Marom, *J. Neurosci.*, 2001, **21**, 8782–8788.
24 P. Massobrio, J. Tessadori, M. Chiappalone and M. Ghirardi, *Neural Plast.*, 2015, **2015**, 1–18.
25 S. Ostojic, N. Brunel and V. Hakim, *J. Neurosci.*, 2009, **29**, 10234–10253.
26 P. Andersen, H. Silfvenius, S. H. Sundberg, O. Sveen and H. Wigström, *Brain Res.*, 1978, **144**, 11–18.
27 J. L. Novak and B. C. Wheeler, *J. Neurosci. Methods*, 1988, **23**, 149–159.
28 M. V. Kopanitsa, N. O. Afinowi and S. G. N. Grant, *BMC Neurosci.*, 2006, **7**, 1–19.
29 C. Stangl and P. Fromherz, *Eur. J. Neurosci.*, 2008, **27**, 958–964.
30 Q. Qing, S. K. Pal, B. Tian, X. Duan, B. P. Timko, T. Cohen-Karni, V. N. Murthy and C. M. Lieber, *Proc. Natl. Acad. Sci. U. S. A.*, 2010, **107**, 1882–1887.
31 J. T. Robinson, M. Jorgolli, A. K. Shalek, M.-H. H. Yoon, R. S. Gertner and H. Park, *Nat. Nanotechnol.*, 2012, **7**, 180–184.
32 J. Abbott, T. Ye, L. Qin, M. Jorgolli, R. S. Gertner, D. Ham and H. Park, *Nat. Nanotechnol.*, 2017, **12**, 460–466.
33 J. Abbott, T. Ye, K. Krenek, R. S. Gertner, S. Ban, Y. Kim, L. Qin, W. Wu, H. Park and D. Ham, *Nat. Biomed. Eng.*, 2020, **4**, 232–241.

34 J. Abbott, T. Ye, K. Krenek, L. Qin, Y. Kim, W. Wu, R. S. Gertner, H. Park and D. Ham, *IEEE J. Solid-State Circuits*, 2020, 1–1.
35 J. Liu, T. M. Fu, Z. Cheng, G. Hong, T. Zhou, L. Jin, M. Duvvuri, Z. Jiang, P. Kruskal, C. Xie, Z. Suo, Y. Fang and C. M. Lieber, *Nat. Nanotechnol.*, 2015, **10**, 629–635.
36 G. Hong and C. M. Lieber, *Nat. Rev. Neurosci.*, 2019, **20**, 330–345.
37 E. Musk and Neuralink, bioRxiv, 2019, p. 703801.
38 E. R. McConnell, M. A. McClain, J. Ross, W. R. LeFew and T. J. Shafer, *NeuroToxicology*, 2012, **33**, 1048–1057.
39 R. A. Nicoll, *Neuron*, 2017, **93**, 281–290.
40 J. C. Magee and C. Grienberger, *Annu. Rev. Neurosci.*, 2020, **43**, 95–117.
41 J. Scholvin, J. P. Kinney, J. G. Bernstein, C. Moore-Kochlacs, N. Kopell, C. G. Fonstad and E. S. Boyden, *IEEE Trans. Biomed. Eng.*, 2016, **63**, 120–130.
42 G. J. Augustine, M. P. Charlton and S. J. Smith, *Annu. Rev. Neurosci.*, 1987, **10**, 633–693.
43 I. Parnas, H. Parnas and J. Dudel, *Pflügers Arch.*, 1982, **395**, 261–270.
44 D. A. Wagenaar, J. Pine and S. M. Potter, *J. Neurosci. Methods*, 2004, **138**, 27–37.
45 S. O. Rizzoli and W. J. Betz, *Nat. Rev. Neurosci.*, 2005, **6**, 57–69.
46 S. O. Rizzoli, *EMBO J.*, 2014, **33**, 788–822.
47 M. Andreasen, J. D. Lambert and M. S. Jensen, *J. Physiol.*, 1989, **414**, 317–336.

